Nano-scale stabilization of sodium oxides: Implications for Na-O_2 batteries

ShinYoung Kang,[a] Yifei Mo,[b] Shyue Ping Ong,[c] and Gerbrand Ceder[a]*

[a] Department of Materials Science and Engineering, Massachusetts Institute of Technology, Cambridge, Massachusetts 02139, USA

[b] Current address: Department of Materials Science and Engineering, University of Maryland, College Park, MD 20742, USA

[c] Current address: Department of NanoEngineering, University of California, San Diego, La Jolla, CA 92093, USA

Supporting Information

1. Phase information about Na−O compounds

Experimentally reported stability ranges of Na−O compounds considered in this study are summarized in Table S 1.[1-3] Since the $P6_3/mmc$ structure of Na metal is only stable below 36 K, and the $Im\bar{3}m$ structure is stable between 36 and 370.98 K, we only considered the $Im\bar{3}m$ structure for Na metal.

Table S 1. Structure and phase transition information of Na and Na−O compounds considered in this study.

Compound	Structure	Note
Na	$P6_3/mmc$	Phase transition from $P6_3/mmc$ to $Im\bar{3}m$ at ~ 36 K
	$Im\bar{3}m$	Melting at 370.98 K
Na_2O	$Fm\bar{3}m$	Stable up to 1407 K
Na_2O_2	$P\bar{6}2m$	Phase transition to a different structure at ~785 K
NaO_2	Pnnm	Magnetic transition at ~ 43 K, Phase transition from Pnnm to ordered $Pa\bar{3}$ at 196 K
	$Pa\bar{3}$	O_2 bonds aligned to <111> directions, Order-disorder transition at 223 K
	$Fm\bar{3}m$	Disordered arrangements of O_2 bonds
NaO_3	Imm2 (I4/mmm)	Wriedt[1] reported on I4/mmm structure, but all compounds reported in ICSD (ICSD # 85587, 180566, 411168) are in the Im2m structure.

2. Computational details for phonon calculations and results

The supercell dimensions used for phonon computation were as follows: 5 × 5 × 5 for $Im\bar{3}m$ Na, 4 × 4 × 4 for $Fm\bar{3}m$ Na_2O, 2 × 2 × 3 for $P\bar{6}2m$ Na_2O_2, 3 × 3 × 3 for Pnnm NaO_2, 3 × 3 × 3 for $R\bar{3}m$ NaO_2 (to represent $Fm\bar{3}m$ NaO_2), and 3 × 3 × 3 for Imm2 NaO_3. For each compound, 0.04 Å of symmetrically distinct atomic displacements were introduced, and the Hellman-Feynman forces were obtained in GGA-DFT.

The Gibbs free energy of solids is approximated by the Helmholtz free energy as

$$\begin{aligned} G(T,P) &\cong F(T,V^0) \\ &= E^{\text{total}}(V^0) + \Delta F^{\text{harm}}(T,V^0) \\ &= E^{\text{total}}(V^0) + \Delta E^{\text{harm}}(T,V^0) - TS^{\text{harm}}(T,V^0), \end{aligned} \qquad \text{Eq. S (1)}$$

where V^0 is the optimized volume of the solid within DFT, $\boldsymbol{E}^{\text{total}}$ is the total energy calculated in DFT, ΔF^{harm} is the Helmholtz free energy change due to vibrations in the harmonic approximation

The phonon spectra calculated for Na metal and Na−O compounds are displayed in Figs. S 1−7. Due to the presence of imaginary frequencies in Pa$\bar{3}$ NaO_2 (ordered form of Fm$\bar{3}$m NaO_2) in Fig. S 5, we have tested different sets of energy and force convergence criteria, kinetic energy cutoff, charge density mixing parameters, and algorithms that can influence the final structure and Hellman-Feynman forces within the small displacement method we used. In addition, we have calculated the phonon spectra using the density functional perturbation theory.[4-6] However, none of these attempts were successful in removing the imaginary frequencies. In Fig. S 5, we show the phonon dispersion and density of states (DOS) of Pa$\bar{3}$ NaO_2 calculated with the small displacement method with an energy cutoff of 700 eV, and the density functional perturbation theory using VASP. In both methods, the phonon spectra of Pa$\bar{3}$ NaO_2 show imaginary frequencies indicating that the Pa$\bar{3}$ NaO_2 structure is not dynamically stable.

Instead, we performed phonon calculations on the Rm$\bar{3}$ NaO_2 structure, whose phonon dispersion and phonon DOS are displayed in Fig. S 6. In addition to the phonon vibrational energy and entropy of Rm$\bar{3}$ NaO_2, the energy and entropy of rigid rotors are added to calculate the Gibbs free energy of disordered Fm$\bar{3}$m NaO_2 as a function of temperature;

$$\boldsymbol{E}^{\text{rotor}} \approx \boldsymbol{k_B T}\left\{1-\frac{\boldsymbol{T}_{\text{rot}}}{3\boldsymbol{T}}-\frac{1}{45}\left(\frac{\boldsymbol{T}_{\text{rot}}}{\boldsymbol{T}}\right)^2\right\} \text{ and } \boldsymbol{S}^{\text{rotor}} \approx \boldsymbol{k_B}\left\{1-\ln\left(\frac{2\boldsymbol{T}_{\text{rot}}}{\boldsymbol{T}}\right)-\frac{1}{90}\left(\frac{\boldsymbol{T}_{\text{rot}}}{\boldsymbol{T}}\right)^2\right\} \quad \text{Eq. S (2)}$$

per O_2, when $T > 5\,\boldsymbol{T}_{\text{rot}}$. $\boldsymbol{k_B}$ is the Boltzmann constant, and $\boldsymbol{T}_{\text{rot}}$ =2.08 K is the characteristic rotational temperature of O_2 gas. The degree of contribution of the rigid rotor to the free energy was set to 80% to reproduce the phase transition temperature between the NaO_2 polymorphs, and the equilibrium temperature between Na_2O_2 and NaO_2 at P_{O_2} = 1 atm.

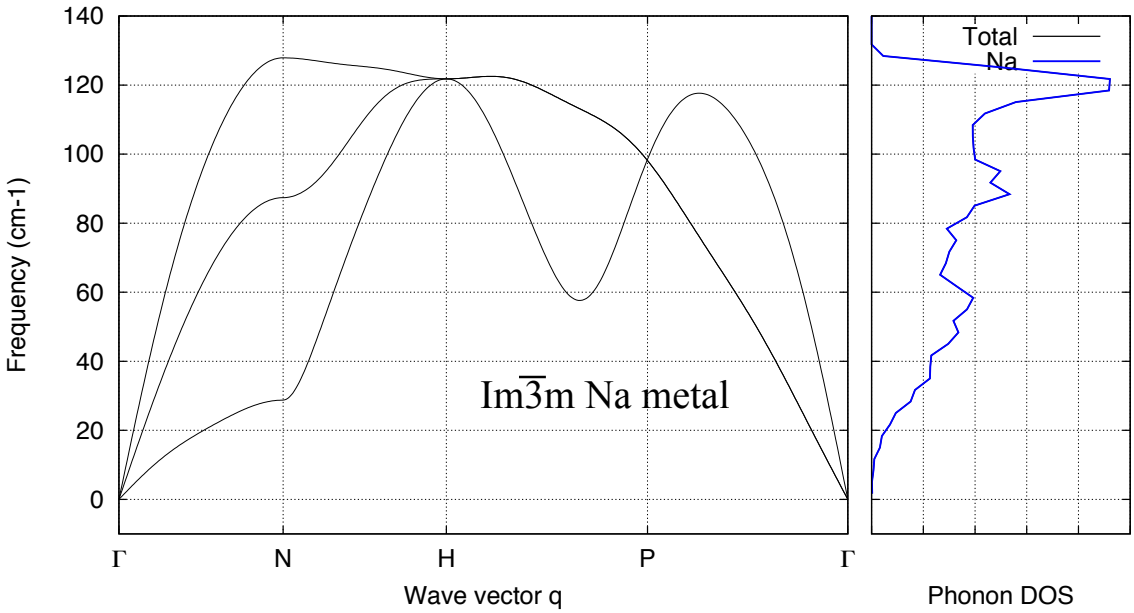

Fig. S 1. Phonon dispersion and density of states for Im $\bar{3}$ m Na metal.

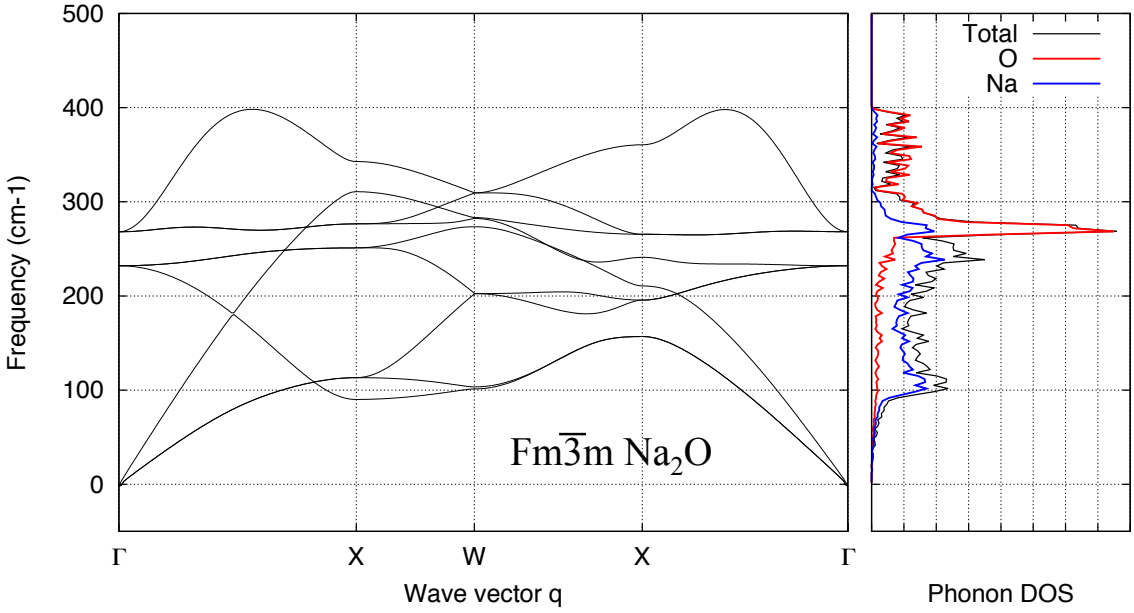

Fig. S 2. Phonon dispersion and density of states for Fm $\bar{3}$ m Na_2O. The partial phonon density of states contributed from Na and O are shown in blue and red, respectively.

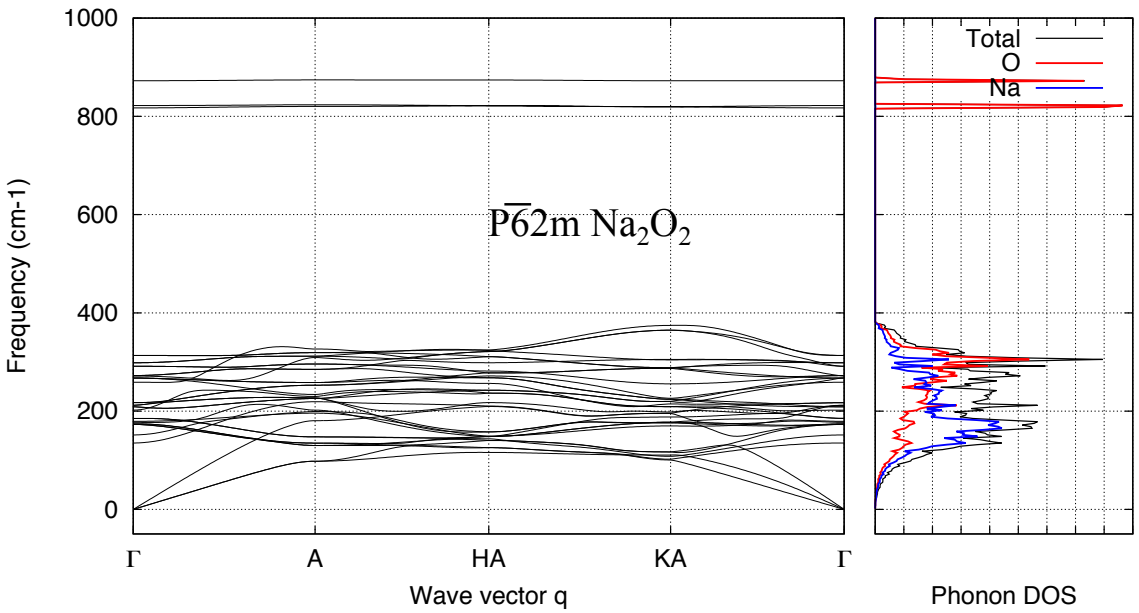

Fig. S 3. Phonon dispersion and density of states for P$\bar{6}$2 Na_2O_2. The partial phonon density of states contributed from Na and O are shown in blue and red, respectively.

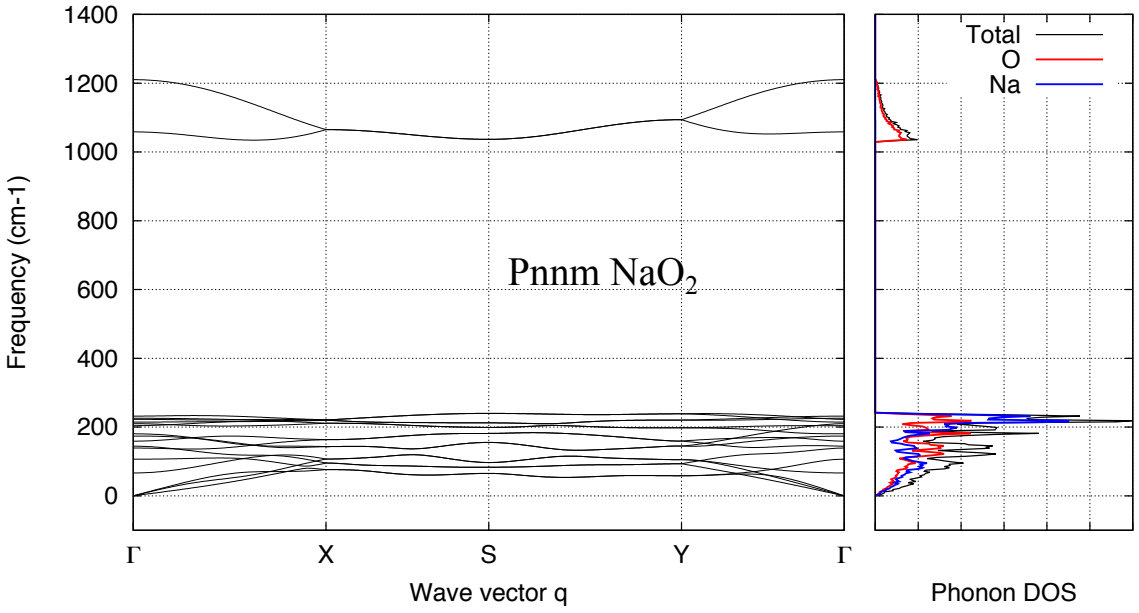

Fig. S 4. Phonon dispersion and density of states for Pnnm NaO_2. The partial phonon density of states contributed from Na and O are shown in blue and red, respectively.

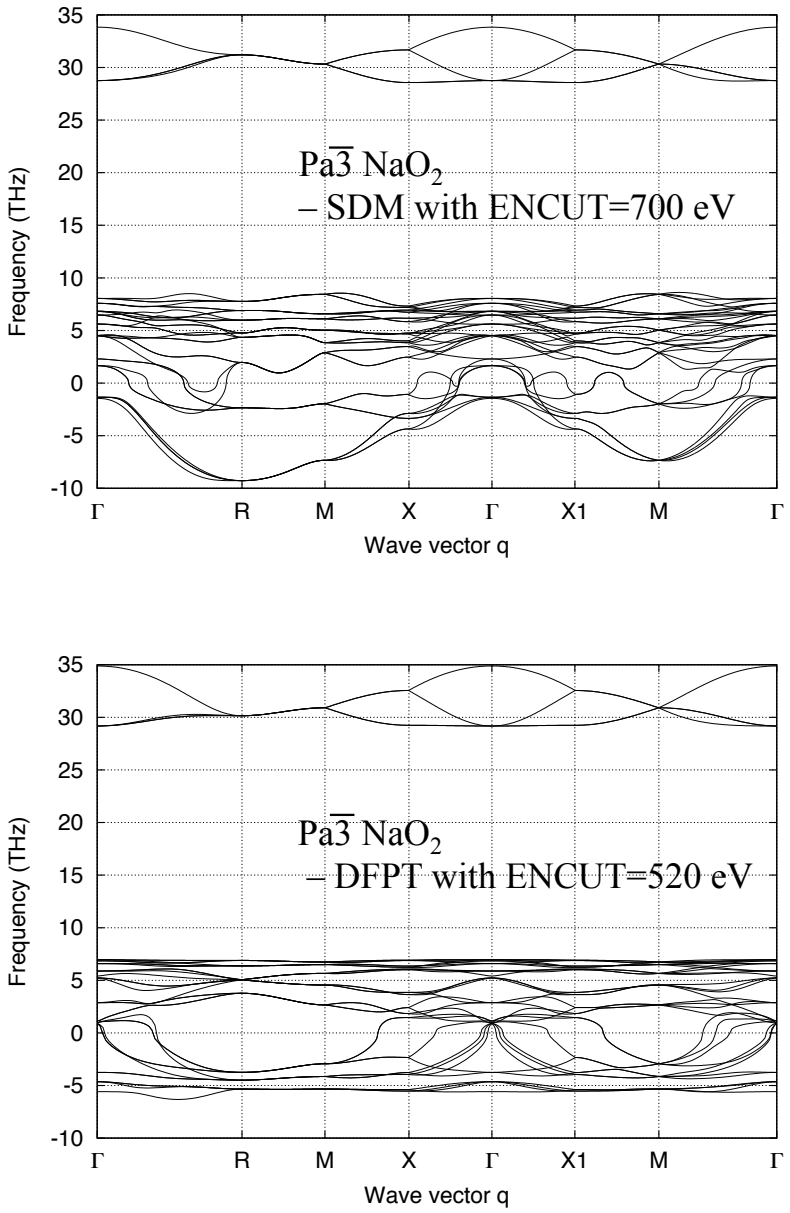

Fig. S 5. Phonon dispersion and density of states for Pa$\bar{3}$ NaO_2 calculated in small displacement method (SDM) with energy cutoff set to 700 eV (top) and the density functional perturbation theory (DFPT, bottom).

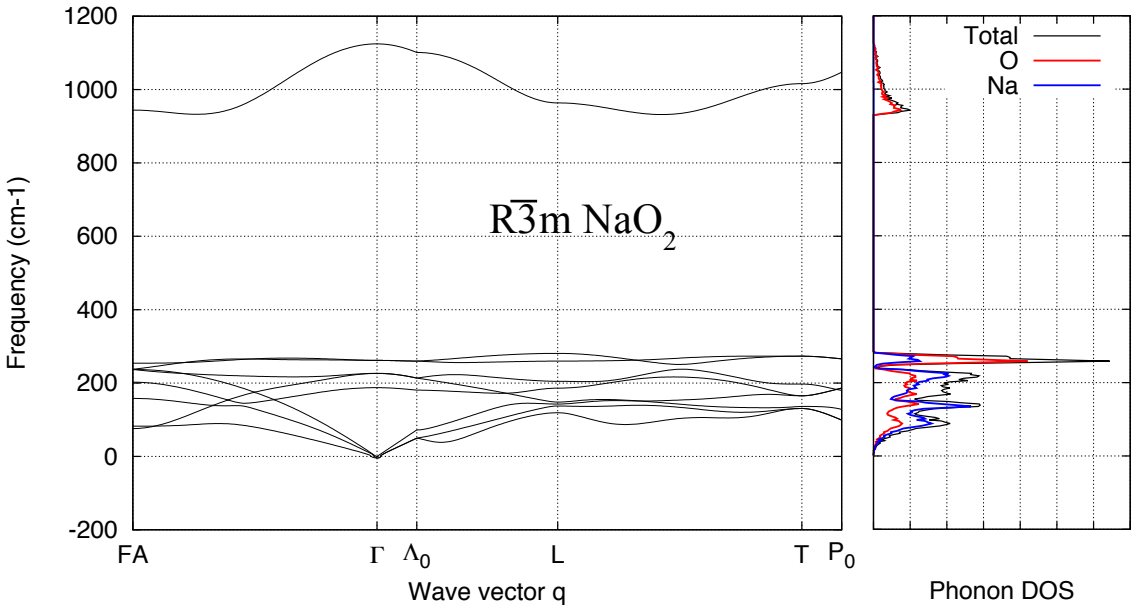

Fig. S 6. Phonon dispersion and density of states for R $\bar{3}$ m NaO_2. The partial phonon density of states contributed from Na and O are shown in blue and red, respectively.

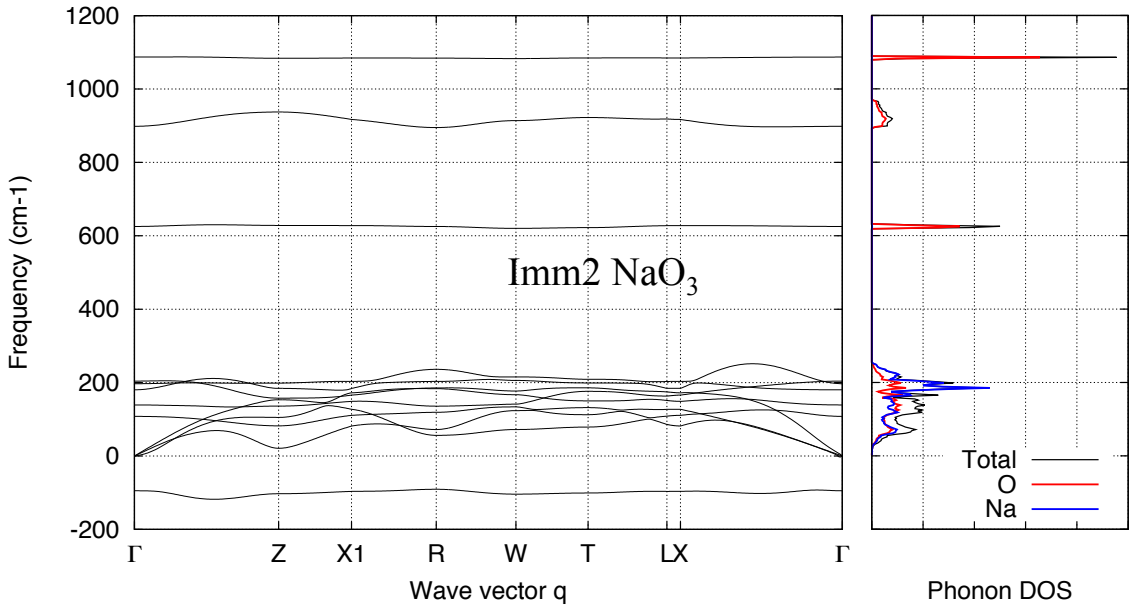

Fig. S 7. Phonon dispersion and density of states for Imm2 NaO_3. The partial phonon density of states above 0 cm^{-1} are plotted, and the contribution of Na and O are shown in blue and red, respectively. The phonon spectra of NaO_3 in Imm2 structure revealed imaginary frequencies indicating the NaO_3 phase is not dynamically stable.

3. Formalism for the temperature and O_2 partial pressure dependent formation free energy

The formation enthalpy of Na−O compounds at 300 K can be expressed by combining Eq. (1) and the oxidation energy correction term as

$$\Delta \boldsymbol{H}_{\text{form}}(300\ \text{K}) = \Delta \boldsymbol{E}_{\text{form}}(0\ \text{K}) - \tfrac{y}{2}\boldsymbol{E}_{\text{oxd}} \quad \text{Eq. S (3)}$$

Referencing to the formation enthalpy at 300 K, $\Delta \boldsymbol{H}_{\text{form}}$ at a given temperature T can be calculated as

$$\begin{aligned}\Delta \boldsymbol{H}_{\text{form}}(\boldsymbol{T}) &= \Delta \boldsymbol{H}_{\text{form}}(300\ \text{K}) + \left\{ \boldsymbol{E}^{\text{harm}}_{\text{Na}_x\text{O}_y}(\boldsymbol{T}) - \boldsymbol{x}\boldsymbol{E}^{\text{harm}}_{\text{Na}}(\boldsymbol{T}) - \tfrac{y}{2}\Delta \boldsymbol{H}_{\text{O}_2}(\boldsymbol{T}) \right\} \\ &\quad - \left\{ \boldsymbol{E}^{\text{harm}}_{\text{Na}_x\text{O}_y}(300\ \text{K}) - \boldsymbol{x}\boldsymbol{E}^{\text{harm}}_{\text{Na}}(300\ \text{K}) - \tfrac{y}{2}\Delta \boldsymbol{H}_{\text{O}_2}(300\ \text{K}) \right\} \\ &= \Delta \boldsymbol{H}_{\text{form}}(300\ \text{K}) + \Delta\Delta \boldsymbol{H}_{\text{form}}(\boldsymbol{T}) - \Delta\Delta \boldsymbol{H}_{\text{form}}(300\ \text{K}) \end{aligned}, \quad \text{Eq. S (4)}$$

where $\boldsymbol{E}^{\text{harm}}_{\boldsymbol{i}}$ is the internal energy of solid *i* contributed from the phonon vibration as in Eq. (2), $\Delta \boldsymbol{H}_{\text{O}_2}(\boldsymbol{T}) = \tfrac{7}{2}\boldsymbol{k}_{\boldsymbol{B}}\boldsymbol{T}$ using the diatomic ideal gas approximation for the enthalpy of O_2 gas, and $\Delta\Delta \boldsymbol{H}_{\text{form}}$ is defined as

$$\Delta\Delta \boldsymbol{H}_{\text{form}}(\boldsymbol{T}) \equiv \boldsymbol{E}^{\text{harm}}_{\text{Na}_x\text{O}_y}(\boldsymbol{T}) - \boldsymbol{x}\boldsymbol{E}^{\text{harm}}_{\text{Na}}(\boldsymbol{T}) - \tfrac{y}{2}\Delta \boldsymbol{H}_{\text{O}_2}(\boldsymbol{T}) \quad \text{Eq. S (5)}$$

In the same way, the formation free energy of Na−O compounds at 300 K and 1 atm can be expressed as

$$\begin{aligned}&\Delta \boldsymbol{G}_{\text{form}}(300\ \text{K},\ 1\ \text{atm}) \\ &\quad = \Delta \boldsymbol{H}_{\text{form}}(300\ \text{K}) - 300 \cdot \Delta \boldsymbol{S}_{\text{form}}(300\ \text{K},\ 1\ \text{atm}) \\ &\quad = \left\{ \Delta \boldsymbol{E}_{\text{form}}(0\ \text{K}) + \tfrac{y}{2}\boldsymbol{E}_{\text{oxd}} \right\} - 300 \cdot \Delta \boldsymbol{S}_{\text{form}}(300\ \text{K},\ 1\ \text{atm}) \end{aligned}, \quad \text{Eq. S (6)}$$

and can be generalized to any given temperature and O_2 partial pressure as

$$\begin{aligned}\Delta G_{\text{form}}(T, P_{\text{O}_2}) &= \Delta H_{\text{form}}(T) - T\Delta S_{\text{form}}\left(T, P_{\text{O}_2}\right) \\ &\cong \Delta H_{\text{form}}(300\ \text{K}) + \Delta\Delta H_{\text{form}}(T) - \Delta\Delta H_{\text{form}}(300\ \text{K}) \\ &\quad - T\left\{ S^{\text{harm}}_{\text{Na}_x\text{O}_y}(T, V^0_{\text{Na}_x\text{O}_y}) - xS^{\text{harm}}_{\text{Na}}(T, V^0_{\text{Na}}) - \tfrac{y}{2}S_{\text{O}_2}\left(T, P_{\text{O}_2}\right) \right\}. \end{aligned} \quad \text{Eq. S (7)}$$

Note that we approximated the formation entropy $\Delta \boldsymbol{S}_{\text{form}}$ by the formation entropy using the phonon vibrational entropy for solids.

$$\Delta \boldsymbol{S}_{\text{form}} = \boldsymbol{S}^{\text{harm}}_{\text{Na}_x\text{O}_y} - \boldsymbol{x}\boldsymbol{S}^{\text{harm}}_{\text{Na}} - \tfrac{y}{2}\boldsymbol{S}^{\text{expt}}_{\text{O}_2} \quad \text{Eq. S (8)}$$

The entropy of O_2 gas, as described in Eq. (1) in the main text, is obtained by combining experimental entropy[7] and the ideal gas behavior as

$$S_{O_2}(T, P_{O_2}) = S_{O_2}^{expt}(T) - k_B \log\left(P_{O_2} / P_{O_2}^{o}\right) \quad \text{Eq. S (9)}$$

4. Temperature dependent stability of the Na−O compounds

The formation free energies of Na_2O, Na_2O_2, and NaO_2 in eV/Na versus temperature are plotted in Fig. S 8. In Fig. S 8, the solid blue, red, and green lines (circles) represent calculated (experimental) ΔG_{form} of Na_2O, Na_2O_2, and NaO_2, respectively. The green line is obtained as the lowest energy envelope of the two NaO_2 polymorphs, shown as the dashed gray line for Pnnm NaO_2 and the dash-dot gray line for Fm$\bar{3}$m NaO_2. The energy is given per Na in the formula unit to represent the system open to oxygen. Given that the experimental ΔG_{form} at 1 atm are available,[7] the temperature dependency of ΔG_{form} can be used to validate our computations. As can be seen from Fig. S 8, the temperature dependent ΔG_{form} of the Na−O compounds are in good agreement with experimental values. The absolute errors at any given temperature are less than 40 meV/Na. Absolute errors for Na_2O_2 and NaO_2, which are interest as discharge products in Na−O_2 batteries, are less than 30 meV/Na. As these errors are almost constant with respect to temperature (Fig. S 8), the primary source of errors is ΔH_{form}, and we can presumably conclude that the source of errors is the oxidation energy correction that is obtained from the fitting of various metal oxides, peroxides, and superoxides. Although Na_2O_2 is slightly under-stabilized compared to NaO_2, our computational results successfully predict the trends in ΔG_{form} with respect to temperature and the relative stability of Na−O compounds. Thus, we continue our study to investigate the phase stability of Na−O compounds as a function of O_2 partial pressure, as the O_2 partial pressure is a more important parameter that varies during charge and discharge of Na−O_2 batteries.

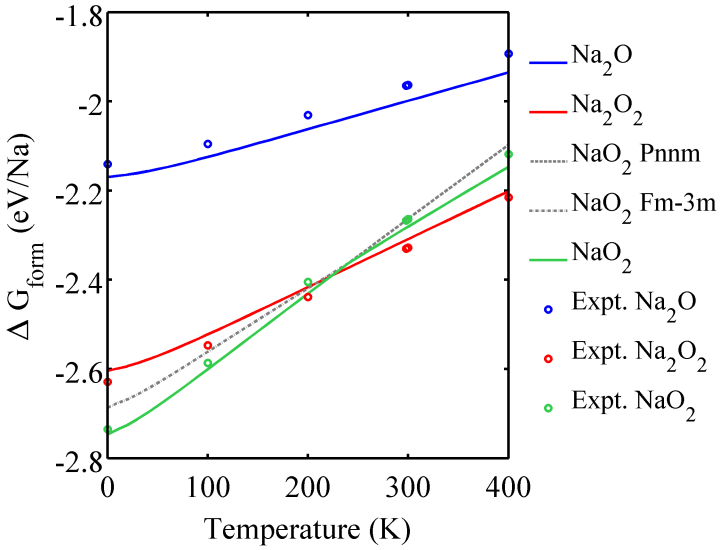

Fig. S 8. The formation free energies of $Fm\bar{3}m$ Na_2O (blue), $P\bar{6}2m$ Na_2O_2 (red), Pnnm NaO_2 (dashed gray line), $Fm\bar{3}m$ NaO_2 (dash-dot gray line), and the lowest energy envelope for NaO_2 (green) as a function of temperature. Calculated data are plotted in lines, and experimental data are marked as circles.

Adding the full rotor energy and entropy contribution to the energy of $Fm\bar{3}m$ overestimates the stability of this phase, as some of this excitation is also counted in the phonon spectrum of the structure. We find that reducing the rotor contribution to 80% best reproduces transition temperatures between Na_2O_2 and NaO_2, and between Pnnm NaO_2 and $Fm\bar{3}m$ NaO_2. With this approximation, the transition temperature from Pnnm NaO_2 to $Fm\bar{3}m$ NaO_2 is between 230 and 240 K in our calculations, in fair agreement with experimental transition temperatures that are 196 K from Pnnm to ordered $Pa\bar{3}$, and 223 K from ordered $Pa\bar{3}$ to $Fm\bar{3}m$.[2, 3] In addition, the equilibrium temperature between NaO_2 and Na_2O_2 is calculated at 210−220 K, while it is located at between 100 K and 200 K in experiment.[1] To our knowledge, the exact temperature has not been reported.

5. Chemical potentials of Na and O at Na−O phase boundaries

The chemical potential of Na in Na_xO_2 (x = 1 or 2) is limited on the upper end by the chemical potential of Na metal and at the lower end by the decomposition of Na_xO_2:

$$\mu_{\mathrm{Na}}^{\text{Na metal}}(T)+\frac{1}{x}\Delta G_{\text{form}}^{\mathrm{Na}_x\mathrm{O}_2}\left(T,P_{\mathrm{O}_2}\right) < \mu_{\mathrm{Na}}^{\mathrm{Na}_x\mathrm{O}_2}\left(T,P_{\mathrm{O}_2}\right) < \mu_{\mathrm{Na}}^{\text{Na metal}}(T) \quad \text{Eq. S (10)}$$

where μ_{O} is set to the energy of O_2 gas per atom. We defined the chemical potentials of Na or O at the phase boundaries where the two phases are in equilibrium. For example, μ_{Na} in Na_2O_2 at the Na_2O limit is calculated as

$$\mu_{\mathrm{Na}}^{\mathrm{Na}_2\mathrm{O}_2/\mathrm{Na}_2\mathrm{O}}\left(T,P_{\mathrm{O}_2}\right)=\mu_{\mathrm{Na}}^{\text{Na metal}}(T)+\frac{1}{2}\left\{2\Delta G_{\text{form}}^{\mathrm{Na}_2\mathrm{O}}\left(T,P_{\mathrm{O}_2}\right)-\Delta G_{\text{form}}^{\mathrm{Na}_2\mathrm{O}_2}\left(T,P_{\mathrm{O}_2}\right)\right\}, \quad \text{Eq. S (11)}$$

which results in $\mu_{\mathrm{Na}} = -3.08$ eV and $\mu_{\mathrm{O}} = -5.82$ eV. The chemical potentials of Na and O at phase boundaries at 300 K and 1 atm are denoted in Fig. S 9.

The thermodynamically stable regime of bulk Na_2O_2 is restricted within the O_2 gas and the Na_2O limits, representing the most oxidizing and reducing conditions, respectively. The formation of bulk NaO_2 is never thermodynamically stabilized at 300 K and 1 atm, and it is formed within the O_2 gas and Na_2O_2 limits most likely, representing the most oxidizing and reducing conditions, respectively. The T−P_{O_2} phase diagram displayed in Fig. 3 is obtained at the O_2 gas limit where $\mu_{\mathrm{O}} = -5.20$ eV at 300 K and 1 atm..

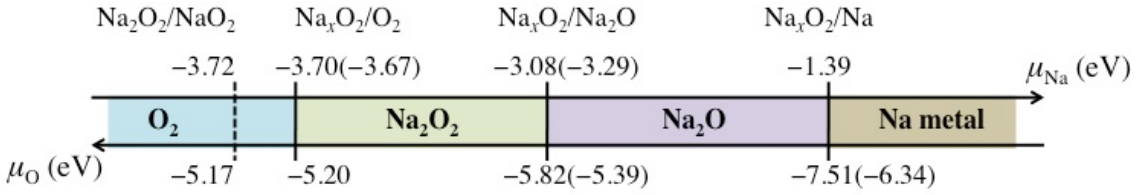

Fig. S 9. The chemical potentials of Na and O when Na_xO_2 (x = 1 or 2) is in equilibrium with the corresponding phase. When μ_{Na} and/or μ_{O} are different for Na_2O_2 and NaO_2 at the phase boundaries, the values corresponding to NaO_2 are marked in parentheses.

6. Surface energy calculations

The surface energies of Na_2O_2 and Pa$\bar{3}$ NaO_2 are calculated using the surface slab method.[8, 9] The vacuum layers in the surface slabs were at least 10 Å, and the Na_xO_2 ($x = 1$ or 2) compound layers were ~20 Å thick. The same energy cutoff, energy and force convergence criteria, and *k*-points sampling settings were used as for the bulk energy calculations.

We considered 16, 17, and 5 terminations for the {0001}, {1$\bar{1}$00}, and {11$\bar{2}$0} surface orientations of Na_2O_2, respectively, and 3, 1, 1, and 2 terminations for the {100}, {110}, {111}, and {211} surface orientations of Pa$\bar{3}$ NaO_2, respectively. The (T, $\boldsymbol{P}_{O_2}$)-dependent surface energy formalism is adopted from Reuter and Scheffler.[9]

Based on the calculated surface energies, we constructed the Wulff shapes at the oxidizing and reducing phase boundaries of Na_xO_2 ($x = 1$ or 2). At the most oxidizing condition (O_2 gas limit) of Na_2O_2, the Wulff shape of Na_2O_2 is a dodecagonal prism that is composed of the {0001}, {1$\bar{1}$00}, and {11$\bar{2}$0} surface orientations. The normalized total surface energies $\bar{\gamma}$ at this condition is calculated as 0.178 eV/Å^3. At the most reducing condition (Na_2O limit) of Na_2O_2, the {1$\bar{1}$00} facets disappear and the {0001} and {11$\bar{2}$0} facets form a hexagonal prism Wulff shape for Na_2O_2 with $\bar{\gamma}$ = 0.196 eV/Å^3. Due to the absence of experimental observation of Na_2O_2 particle shapes (to our knowledge), comparison of predicted Wulff shapes with experiments was not possible.

On the other hand, the Wulff shape of Pa$\bar{3}$ NaO_2 is cubic at both the most oxidizing (O_2 gas limit) and reducing (Na_2O_2 limit) conditions. The lowest energy {100} facets were stoichiometric, resulting in $\bar{\gamma}$ = 0.070 eV/Å^3 at both the most oxidizing and reducing conditions.

7. Formalism for particle size dependent formation free energy of Na_xO_2

The formation energy of a particle with unit volume (1 Å^3) is calculated as

$$\begin{aligned}\Delta\bar{G}_{\text{form}}\left(T,P_{O_2}\right) &= \Delta G^{\text{bulk}}_{\text{form}}\left(T,P_{O_2}\right)\cdot V_1 + \sum_i \gamma_i\left(T,P_{O_2}\right)\cdot A_{1,i} \\ &= \Delta G^{\text{bulk}}_{\text{form}}\left(T,P_{O_2}\right) + \sum_i \gamma_i\left(T,P_{O_2}\right)\cdot A_{1,i} \\ &\equiv \Delta G^{\text{bulk}}_{\text{form}}\left(T,P_{O_2}\right) + \bar{\gamma}\left(T,P_{O_2}\right)\end{aligned}, \qquad \text{Eq. S (12)}$$

where $\Delta G^{\text{bulk}}_{\text{form}}$ is the formation energy of bulk Na_xO_2 in eV/Å^3, γ_i is the surface energy of *i* facet in the predicted Wulff shape in eV/Å^2, and $A_{1,i}$ is the surface area of *i* facet for a unit volume particle (V_1 = 1 Å^3) in Å^2. Here we defined the normalized total surface energy $\bar{\gamma}$ as the free energy contributed from surfaces for a particle with a unit volume. The formation energy of a particle with an arbitrary volume V_2 can be calculated as

$$\begin{aligned}\Delta G_{\text{form}}\left(d,T,P_{O_2}\right) &= \Delta G^{\text{bulk}}_{\text{form}}\left(T,P_{O_2}\right)\cdot V_2 + \sum_i \gamma_i\left(T,P_{O_2}\right)\cdot A_{2,i} \\ &\equiv \Delta G^{\text{bulk}}_{\text{form}}\left(T,P_{O_2}\right)\cdot d^3\cdot V_1 + \sum_i \gamma_i\left(T,P_{O_2}\right)\cdot d^2\cdot A_{1,i} \\ &= \Delta G^{\text{bulk}}_{\text{form}}\left(T,P_{O_2}\right)\cdot d^3 + \bar{\gamma}\left(T,P_{O_2}\right)\cdot d^2\end{aligned}, \qquad \text{Eq. S (13)}$$

where A_2 is the the surface area of *i* facet corresponding to the particle volume V_2, and the particle size *d* is defined as $d = (V_2/V_1)^{1/3} = (V_2)^{1/3}$.

8. Formalism for critical nucleus size of Na_2O_2 and Fm $\bar{3}$ m NaO_2 nano-particles and their nucleation energy barrier

We calculated the critical nucleus size using the P_{O_2} and/or the electrochemical potential ϕ as a driving force for nucleation:

$$\Delta G_v\left(T, P_{O_2}, \phi\right) = \frac{\Delta G_{\text{form}}^{Na_xO_2}\left(T, 1\text{ atm}, \phi_{\text{eq}}^{Na_xO_2}\right) + xF\phi - k_B T \ln P_{O_2}}{xV^{Na_xO_2}}, \qquad \text{Eq. S (14)}$$

where $\Delta G_{\text{form}}^{Na_xO_2}$ is the formation free energy of bulk Na_xO_2 at a given temperature T, 1 atm and its equilibrium potential $\phi_{\text{eq}}^{Na_xO_2}$, F is the Faraday constant, and $V^{Na_xO_2}$ is the volume of Na_xO_2 in $Å^3$ per formula unit. The nucleation driving force ΔG_v is the normalized formation free energy of Na_xO_2 at arbitrary P_{O_2} and electrochemical potential ϕ in eV/$Å^3$ per Na. We plugged ΔG_v into $\Delta G_{\text{form}}^{\text{bulk}}$ in Eq. S (13) as follows:

$$\Delta G_{\text{form}}\left(d, T, P_{O_2}, \phi\right) = \Delta G_v\left(T, P_{O_2}, \phi\right)\cdot d^3 + \bar{\gamma}\left(T, P_{O_2}\right)\cdot d^2, \qquad \text{Eq. S (15)}$$

and calculated the size of critical nucleus when $\partial \Delta G_{\text{form}}\left(d, T, P_{O_2}, \phi\right)/\partial d = 0$, resulting in the critical nucleus size and the nucleation energy barrier as

$$d^* = -\frac{2\bar{\gamma}\left(T, P_{O_2}\right)}{3\Delta G_v\left(T, P_{O_2}, \phi\right)}, \text{ and } \Delta G^* = \frac{4\left\{\bar{\gamma}\left(T, P_{O_2}\right)\right\}^3}{27\left\{\Delta G_v\left(T, P_{O_2}, \phi\right)\right\}^2}. \qquad \text{Eq. S (17)}$$

Note that the normalized total surface energies $\bar{\gamma}$ is calculated at the O_2 gas limit where the chemical potential of O_2 is set to −5.20 eV, corresponding to 300 K and 1 atm as in Fig. S 11. While $\bar{\gamma}$ is independent on the O_2 partial pressure P_{O_2} and the potential ϕ, ΔG_v is dependent on them. This leads to overestimation of the nucleation energy barrier at smaller driving force, corresponding to lower P_{O_2} and/or closer to the $\phi_{\text{eq}}^{Na_xO_2}$.

However, otherwise, we expect the ΔG^* will serve as a useful descriptor to assess the feasibility of nucleation.

References

(1) Wriedt, H. A. *Bulletin of Alloy Phase Diagrams* **1987,** 8 (3), 234-246.
(2) Carter, G. F.; Templeton, D. H. *Journal of the American Chemical Society* **1953,** 75 (21), 5247-5249.
(3) Templeton, D. H.; Dauben, C. H. *Journal of the American Chemical Society* **1950,** 72 (5), 2251-2254.
(4) Gonze, X. *Physical Review A* **1995,** 52 (2), 1096-1114.
(5) Gonze, X. *Physical Review A* **1995,** 52 (2), 1086-1095.
(6) Baroni, S.; Giannozzi, P.; Testa, A. *Physical Review Letters* **1987,** 58 (18), 1861-1864.
(7) Chase, M. W.; National Institute of, S.; Technology, *NIST-JANAF thermochemical tables*. American Chemical Society ; American Institute of Physics for the National Institute of Standards and Technology: [Washington, D.C.]; Woodbury, N.Y., 1998.
(8) Ramamoorthy, M.; Vanderbilt, D.; King-Smith, R. D. *Physical Review B* **1994,** 49 (23), 16721-16727.
(9) Reuter, K.; Scheffler, M. *Physical Review B* **2001,** 65 (3), 035406.